Soft Matter

PAPER

Electrostatically driven lipid–lysozyme mixed fibers display a multilamellar structure without amyloid features†

Cite this: *Soft Matter*, 2014, **10**, 840

Ana M. Melo,[a] Luís M. S. Loura,[bc] Fábio Fernandes,[a] José Villalaín,[d] Manuel Prieto[a] and Ana Coutinho*[ae]

Understanding the interactions between anionic lipid membranes and amyloidogenic proteins/peptides is key to elucidate the molecular mechanisms underlying the membrane-driven amyloid fiber formation. Here, hen egg-white lysozyme was used as a model protein to test whether this same process also occurs with non-amyloidogenic lipid-binding proteins/peptides. A complementary set of biophysical techniques was employed to study the structure and dynamics of the lipid–lysozyme mixed fibers produced at a low lipid/protein molar ratio that have been proposed earlier to present "amyloid-like" characteristics. The multilamellar architecture of these elongated mesoscopic structures was established by performing time-resolved Förster resonance energy transfer measurements, at both bulk (ensemble) and single-fiber level. The predominantly oligomeric lysozyme and phospholipids were both found to display significantly decreased lateral mobility when embedded in these mixed fibers. Notably, two-photon microscopy of Laurdan revealed that a pronounced membrane surface dehydration/increased molecular interfacial packing was produced exclusively in these elongated mixed supramolecular fibers present in the highly polymorphic samples. Infrared spectroscopic studies of lysozyme in these samples further showed that this protein did not exhibit a rich β-sheet structure characteristic of amyloid fibrils. These results support the conclusion that negatively charged lipid membranes do not have the general ability to trigger amyloid fibril formation of non-amyloidogenic proteins.

Received 6th October 2013
Accepted 4th November 2013

DOI: 10.1039/c3sm52586d

www.rsc.org/softmatter

Introduction

The aggregation of proteins/peptides on the surface of biological membranes has been receiving growing attention since several studies have reported that (i) lipid/water interfaces can promote the self-assembly of amyloidogenic proteins/peptides into a rich β-sheet structure by acting as two-dimensional conformational catalysts and (ii) these soft interfaces can also be a target of amyloid cytotoxicity.[1,2] In fact, the interaction between these amyloidogenic proteins/peptides and lipid membranes has often been found to result in a strong perturbation of the membrane structure.[1,2] Moreover, the toxicity of the oligomeric intermediate species formed during the amyloidogenic protein/peptide aggregation pathway has been directly correlated with their shared ability to disrupt the biological membranes.[3] The key role played by lipid membranes in triggering amyloidogenic protein/peptide fibrillation depends critically on their chemical and physical properties arising from their lipid composition.[1,4,5] Particularly, several studies have highlighted the importance of the net surface charge of the lipid bilayers, since the initial binding step for several amyloidogenic proteins/peptides to the membranes is often driven by electrostatic interactions.[1,2,4,5] In recent years, the group of Kinnunen has generalized this concept by proposing that membranes containing negatively charged phospholipids can also trigger rapid "amyloid-like" fiber formation of a variety of non-amyloidogenic proteins/peptides, such as cytochrome c, lysozyme, endostatin, among others.[6–9] According to the observation that all non-amyloidogenic proteins/peptides studied contained cationic amino acids or clusters of positively charged residues, the authors suggested that the ability to form amyloid fibers is a generic property shared by all proteins/peptides associating electrostatically to membranes containing acidic phospholipids.[6] In order to evaluate whether this concept can be extended to non-amyloidogenic proteins, we have been using hen egg-white lysozyme as a model protein in our lipid–protein interaction studies. Lysozyme is a small polycationic

[a]*Centro de Química-Física Molecular and Institute of Nanoscience and Nanotechnology, Instituto Superior Técnico, Universidade de Lisboa, Av. Rovisco Pais, 1049-001 Lisboa, Portugal. E-mail: ana.coutinho@ist.utl.pt*

[b]*Faculdade de Farmácia, Universidade de Coimbra, 3000-548 Coimbra, Portugal*

[c]*Centro de Química de Coimbra, 3004-535 Coimbra, Portugal*

[d]*Instituto de Biología Molecular y Celular, Universidad Miguel Hernández, E-03202 Elche-Alicante, Spain*

[e]*Dep. Química e Bioquímica, Faculdade de Ciências, Universidade de Lisboa, Campo Grande, 1749-016 Lisboa, Portugal*

† Electronic supplementary information (ESI) available: Materials and methods including the FRET formalisms; Fig. S1 to S3 and Table S1. See DOI: 10.1039/c3sm52586d

protein (estimated net molecular charge +8e at pH 7.4[10]) that displays a high affinity for anionic phospholipid membranes, since its membrane-binding mechanism is mainly driven by electrostatic interactions.[10–14] As a first step towards testing the proposal made by Kinnunen's group, we have recently studied in great detail the interaction of lysozyme with negatively charged membranes (1-palmitoyl-2-oleoyl-*sn-glycero*-3-phosphocholine (POPC) large unilamellar vesicles (LUVs) containing 20 and 30 mol% of 1-palmitoyl-2-oleoyl-*sn-glycero*-3-phosphoserine (POPS)) using a wide range of lipid-to-protein molar (L/P) ratios.[15] After fluorescently labeling lysozyme with the Alexa488 dye (Lz-A488), we explored the biphasic changes in its fluorescence emission kinetics to retrieve information about the sequential conformational/oligomerization transitions undergone by this conjugated protein upon varying its surface concentration on the liposomes. Using the mean fluorescence lifetime of Lz-A488 as a reporter of its assembly state in the membranes, a three-state cooperative partition model was quantitatively fitted to the lifetime data. Briefly, it was found that upon reaching a critical surface concentration of the conjugated protein in the anionic liposomes, Lz-A488 assembles into quenched oligomers that present a mean fluorescence lifetime shorter than the aqueous and membrane-bound monomeric forms of the fluorescently labeled protein.[15] The ability of lysozyme to form mesoscopic lipid–protein mixed fibers at a low L/P ratio was confirmed in that work by using both confocal and fluorescence lifetime imaging microscopy (FLIM) techniques.[15] These lipid–protein mesoscopic assemblies, which match the "amyloid-like" mixed fibers described earlier by the group of Kinnunen,[6,15] were recently reported to significantly reduce cell viability.[14] In order to gain a deeper knowledge about these structures, we focused our work on studying in detail both their structural and dynamic characteristics at the molecular level using a combined set of different biophysical techniques. First, complementary time-resolved fluorescence resonance energy transfer (FRET) measurements from Lz-A488 to a membrane probe acceptor were made, both at the macroscopic and microscopic levels (ensemble-average liposome and single-fiber studies, respectively), to obtain topological information about their supramolecular organization. Secondly, the lateral dynamics of both components of these fibers (phospholipids and lysozyme) was studied using the fluorescence recovery after photobleaching (FRAP) technique. The impact of lipid–protein mixed fiber formation on the structural organization of the membrane's interface was next evaluated by performing two-photon excitation (2PE) measurements of the generalized polarization (GP) of the fluorescent lipid probe 6-dodecanoyl-2-dimethylaminonaphthalene (Laurdan)[16] at the single-fiber level. Finally, to test whether the formation of these lipid–protein mixed supramolecular assemblies was accompanied by a pronounced structural reorganization of lysozyme (β-sheet formation), infrared (IR) spectroscopy measurements were also made. Collectively, our findings suggest that the lipid–protein mixed fibers studied present a multilamellar structure, whose formation imposes a slow lipid/protein lateral diffusion and a pronounced membrane surface dehydration/increased molecular lipid packing but without inducing a major structural re-arrangement of lysozyme.

Experimental section

Materials

POPC, POPS, 1-palmitoyl-2-oleoyl-*sn-glycero*-3-phospho(1′-*rac*-glycerol) (POPG), 1,2-dioleoyl-*sn-glycero*-3-phosphocholine (DOPC), 1,2-dipalmitoyl-*sn-glycero*-3-phosphocholine (DPPC), 1,2-dioleoyl-*sn-glycero*-3-phosphoethanolamine-*N*-(cap biotinyl) (Biotinyl Cap PE), 1,2-dioleoyl-*sn-glycero*-3-phosphoethanolamine-*N*-(lissamine rhodamine B sulfonyl) (Rh-PE), 1,2-dioleoyl-*sn-glycero*-3-phosphoethanolamine-*N*-(7-nitro-2-1,3-benzoxadiazol-4-yl) (NBD-PE), and 1-palmitoyl-2-{12-[(7-nitro-2-1,3-benzoxadiazol-4-yl)amino]dodecanoyl}-*sn-glycero*-3-phosphoserine (NBD-PS) were obtained from Avanti Polar Lipids (Alabaster, AL). Lysozyme (EC 3.2.1.17) and avidin, both from chicken egg white, sucrose and glucose were purchased from Sigma Chemical Co. (St. Louis, MO). Alexa Fluor 488 SE (carboxylic acid, succinimidyl ester, mixed isomers, and dilithium salt) (A488), succinimidyl 6-(*N*-(7-nitrobenz-2-oxa-1,3-diazol-4-yl)amino) hexanoate (NBD-X, SE), and Laurdan were obtained from Molecular Probes, Invitrogen (Eugene, OR). Other chemicals were of analytical or spectroscopic reagent grade, and were used without any purification. The exact concentration of phospholipid stock solutions was determined by phosphate analysis.[17]

Fluorescent labeling of lysozyme

Lysozyme was covalently labeled with the amine-reactive dyes A488 SE or NBD-X, SE essentially as previously described.[12] The final dye-to-protein molar ratio, D/P, was determined spectrophotometrically using the extinction coefficients of the dyes[18,19] and that of lysozyme.[20]

Preparation of liposomes

LUVs were used in most of the experiments. LUVs containing POPC mixtures with either 20 mol% POPS or POPG were prepared by extrusion through 100 nm pore diameter polycarbonate membranes.[12] The lipid mixtures were hydrated in 20 mM HEPES–KOH, 0.1 mM EDTA, pH 7.4 buffer, except for the IR measurements, in which a D_2O buffer with the same composition was used. Laurdan GP measurements were carried out using multilamellar vesicles (MLVs) or giant unilamellar vesicles (GUVs) which were prepared as previously described.[21] The GUVs used in FRAP measurements were immobilized on microscope chambers using an avidin–biotin interaction.[22] LUVs, MLVs and GUVs containing the adequate fluorescent lipid probe were prepared by co-solubilizing the probe in the lipid mixture at the desired molar ratio prior to solvent evaporation (1 : 400 for Rh-PE and Laurdan, and 1 : 250 for NBD-PE and NBD-PS).

Preparation of the lipid–protein mixed fibers

The lipid–protein mixed supramolecular assemblies formed at a low L/P ratio were obtained by incubating 3 μM lysozyme (unlabeled or fluorescently labeled with A488 SE or NBD-X, SE) with 430 μM POPC : POPS 80 : 20 LUVs (with or without the desired fluorescent probe) under constant magnetic stirring for 2 h. These samples were either directly imaged by confocal laser

scanning microscopy (CLSM) or further centrifuged at 10 000 × *g* for 20 min at room temperature. After applying the supernatants to the Ibidi μ-slide 8-well chambers (Ibidi, Martinsried, Germany), the samples were kept immobile at least for 30 min in the dark to allow for the slow deposition of the material present in the supernatants at the bottom of the chambers, and then used in CLSM, FLIM-FRET, FRAP or 2PE Laurdan GP studies.

Confocal laser scanning microscopy

Two different sets of images (pinhole = 111.4 μm) were simultaneously acquired in different channels with a Leica SP5 TCS confocal inverted microscope (Leica Microsystems CMS GmbH, Manheim, Germany) using a 10× objective (0.4 numerical aperture) (Leica, Germany). In the first channel, reflection images were measured by exciting and collecting emission at the same wavelength ($\lambda = 458$ nm). In the Alexa488 channel, the sample was excited at 488 nm, while emission was collected within the 500–600 nm range.

Laurdan generalized polarization measurements

The GP of Laurdan incorporated on GUVs (1 : 400 mol/mol) prepared with a variable lipid composition or on the mixed lipid–protein fibers was measured in the CLSM described above using 2PE and a 63× water (1.2 numerical aperture) apochromatic objective (Leica, Germany). Laurdan was excited at 780 nm by a Ti:sapphire laser (Spectra-Physics Mai Tai BB, 710–990 nm) and intensity images were recorded simultaneously in the range of 400–460 nm (channel 1, $I_{(400-460)}$) and 470–530 nm (channel 2, $I_{(470-530)}$). GP images were obtained by applying the GP function (eqn (1)) to the images obtained from channel 1 and 2 pixel by pixel:[23]

$$\mathrm{GP}_{\mathrm{micro}} = (I_{(400-460)} - GI_{(470-530)})/(I_{(400-460)} + GI_{(470-530)}) \quad (1)$$

The *G*-factor was introduced to compensate for differences in the efficiency of photon collection in the two channels due to instrumental factors.[23] For more details, see ESI.†

FRAP measurements

FRAP experiments were performed on the mixed fibers (with or without NBD-fluorescently-labeled lysozyme (Lz-NBD) or 1 : 250 mol/mol NBD-PE/NBD-PS) or on the top segment of the upper hemisphere of immobilized POPC GUVs (containing 1 : 250 mol/mol NBD-PE or NBD-PS) using the same confocal microscope and a 63× water objective. In all measurements, NBD was excited and bleached with the 488 nm line of the argon laser and the fluorescence was collected between 500 and 600 nm. An image-based FRAP protocol was applied.[24] For further details, see ESI.†

Macroscopic (bulk) FRET measurements

The samples used in the bulk energy transfer experiments were prepared independently by adding different Lz-A488 concentrations (donor, D) to the liposomes at 430 μM total phospholipid concentration (POPC : POPS 80 : 20 LUVs with or without Rh-PE at an acceptor (A)/lipid molar ratio of 1 : 400 (samples DA and D, respectively)). In all assays, the liposome suspensions were incubated with the protein for at least 1 h at room temperature prior to the time-resolved fluorescence measurements. Fluorescence decay measurements of Lz-A488 were carried out using the time-correlated single-photon timing system described elsewhere.[15,25] The samples were excited at 460 nm and the fluorescence was detected at 515 nm. Details about data analysis are provided in the ESI.†

Microscopic FLIM-FRET measurements

FLIM measurements were performed essentially as described earlier[15] using a Becker & Hickl setup (Berlin, Germany) in combination with the CLSM described above. Lz-A488 present in the lipid–protein supramolecular assemblies (fibers and aggregates) was excited at 760 nm (2PE) and the emission was selected with a 500–530 nm band-pass filter (Chroma Technology Corp., Rockingham, USA). The fluorescence decays of donor (Lz-A488) in the absence (D) and presence of acceptors (DA) were fitted with a biexponential model using the SPCImage software, as previously described.[15] The mixed lipid–protein fiber images were pseudocolor-coded according to the amplitude-weighted mean lifetime of the pixels, $\langle\tau\rangle_1$, given by eqn (S6).† $\langle\tau\rangle_1^{\mathrm{D}}$ and $\langle\tau\rangle_1^{\mathrm{DA}}$ correspond to the mean fluorescence lifetime of the donor in the absence and presence of a membrane probe acceptor, respectively. Intensity-weighted frequencies are plotted in the lifetime histograms and therefore the pixels with a higher number of counts have a stronger contribution to the histogram. The FRET efficiency calculated for the mixed fibers using the FLIM measurements, $E_{\mathrm{FRET}}^{\mathrm{FLIM}}$, was obtained using eqn (S7).†

Infrared spectroscopy

The samples for IR spectroscopy were prepared by adding 70 μM of lysozyme in D_2O buffer to 10 mM POPC : POPG 80 : 20 LUVs. Although a much higher protein concentration was used in these samples due to the lower sensitivity of this technique, the L/P molar ratio of the sample was kept constant. After incubating for 2 h under constant magnetic stirring, the suspension was centrifuged. To minimize the contribution of free protein to the IR spectra, the pellet resuspended in D_2O buffer was now used in the IR measurements. As a control, IR spectra of lysozyme and POPC : POPG 80 : 20 LUVs in D_2O buffer were also acquired. The IR spectra were obtained using a Bruker IFS55 spectrometer (Bruker, Ettlingen, Germany) using a deuterated triglycine sulfate detector as previously described.[26,27] For further details, see ESI.†

Results and discussion

FLIM-FRET studies show that the lipid–protein mixed fibers display a multilayer structure at the molecular level

The aim of this study was to obtain both structural and lateral dynamic information about the lipid–protein fibers produced upon lysozyme interaction with anionic lipid membranes at a low L/P ratio and using a low ionic strength buffer[6,15] in order to investigate their "amyloid-like" features. In agreement with our

previous report, micron-sized mesoscopic lipid–protein supramolecular assemblies were produced upon incubating 3 μM Lz-A488 with 430 μM POPC : POPS 80 : 20 LUVs under constant magnetic stirring. Using CLSM, these highly pleomorphic supramolecular assemblies were found to contain both lipid–protein fibers (long narrowed folded structures) and morphologically distinct (irregularly shaped) large aggregates, which greatly differed in size and shape (Fig. 1).[15] To evaluate whether the fluorescently labeled protein is sandwiched between two lipid leaflets in these elongated mesoscopic structures, FLIM-FRET measurements between Lz-A488 (D, donor) and Rh-PE (A, acceptor) were performed at the single-fiber level, which were then compared with equivalent time-resolved fluorescence data obtained under macroscopic (bulk) conditions. After performing a centrifugation step to facilitate the imaging of the samples, the amplitude-weighted mean fluorescence lifetime of Lz-A488 measured by FLIM was found to present a rather uniform spatial distribution in these fibers, with the mean value of the histograms decreasing from $\langle\tau\rangle_1^{\mathrm{D}} = (1.67 \pm 0.13)$ ns to $\langle\tau\rangle_1^{\mathrm{DA}} = (1.06 \pm 0.04)$ ns in the presence of the acceptor (Fig. 2C and D). The FRET efficiency calculated by the FLIM technique, $E_{\mathrm{FRET}}^{\mathrm{FLIM}}$, at the single-fiber level using eqn (S7)† was therefore 0.36 ± 0.03 ($n = 3$). Identical results were obtained for the less-structured aggregates ($E_{\mathrm{FRET}}^{\mathrm{FLIM}} = 0.35 \pm 0.02$, $n = 2$) (Fig. S1 and Table S1†).

The FLIM technique, in which CLSM is combined with fluorescence decay acquisition over a section of an image, yields spatial resolution to the study. In addition, this is an intensity-independent technique that is much less sensitive to artifacts that can potentially interfere with intensity-based microscopic FRET measurements. However, due to low photon counts in each decay (pixel), and thus poor statistics, it is not possible to fit complex FRET topological models to the experimental data. To overcome this limitation, the fluorescence decay kinetics of Lz-A488 in the absence and in the presence of acceptors was also measured under macroscopic (bulk) conditions (*cuvette* measurements). According to the cooperative partition model used earlier to describe the interaction of Lz-A488 with anionic lipid membranes, there was always a significant fraction of free Lz-A488 in solution, $x_{\mathrm{D}}^{\mathrm{w}}$.[15] In fact, considering oligomers with $k = 6$ subunits and a surface aggregation constant, K_{ag}, of 2×10^{14},[15] $x_{\mathrm{D}}^{\mathrm{w}}$ was found to progressively decrease from 0.36 to 0.23 upon varying the Lz-A488 concentration from 1.0 to 3.0 μM

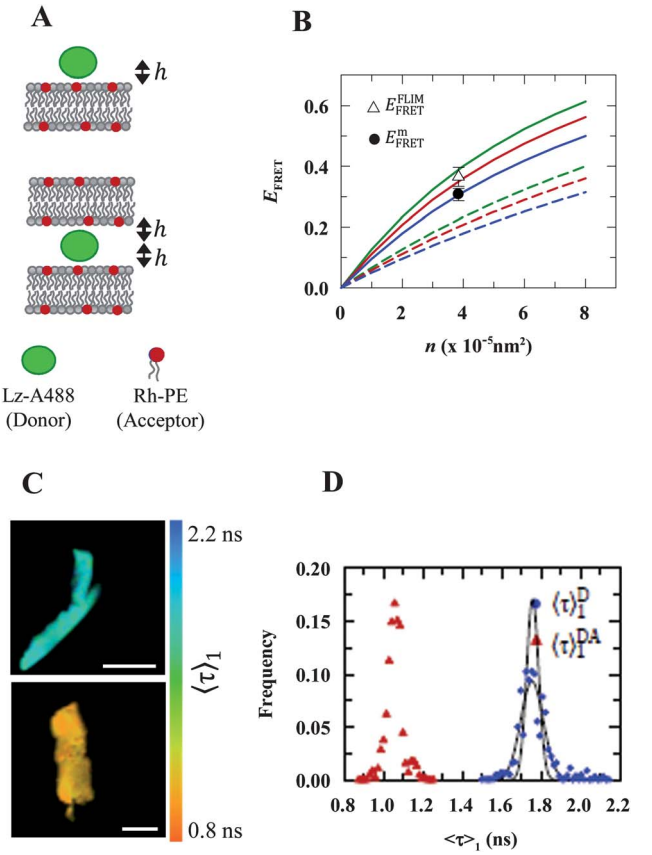

Fig. 2 The lipid–protein mixed fibers display a multilayer structure as revealed by FRET measurements. (A) Schematic representation of the interplanar FRET topological models used in this study. Two donor–acceptor arrangements were considered: FRET between Lz-A488 (donor) to one (top panel) or two (bottom panel) Rh-PE (acceptor) planes, where h is the donor–acceptor interplanar distance. (B) The average experimental FRET efficiencies measured both at the macroscopic ($E_{\mathrm{FRET}}^{\mathrm{m}}$) and single fiber ($E_{\mathrm{FRET}}^{\mathrm{FLIM}}$) levels agree with the theoretical expectation obtained using the multilayer FRET topological model. The FRET efficiencies for the different acceptor surface densities, n, were simulated using eqn (S10)–(S12)† and an interplanar distance of $h = 2.5$ nm (green), $h = 3.0$ nm (red) and $h = 3.5$ nm (blue), respectively. The acceptor numerical density, C (eqn (S11)†) was doubled in the multilayer (solid lines) relatively to the single bilayer (dashed lines) FRET model. (C) Representative images of FLIM-FRET measurements at the single-fiber level (scale bars represent 25 μm). Mean fluorescence lifetime (FLIM) images of Lz-A488 in the absence (D, top panel) and presence of acceptors (DA, bottom panel). (D) Corresponding mean fluorescence lifetime histograms of the D- and DA-containing mixed lipid–protein fibers, respectively.

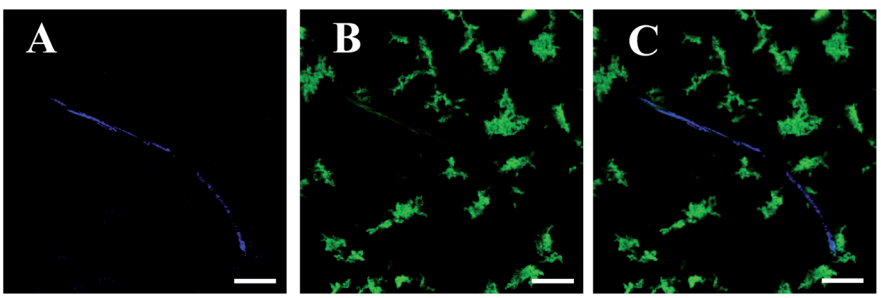

Fig. 1 Confocal laser scanning microscopy of the lipid–protein mixed supramolecular assemblies (fibers and aggregates) formed at a low L/P ratio. (A) Reflection channel in blue ($\lambda_{\mathrm{exc}} = \lambda_{\mathrm{em}} = 458$ nm), (B) Alexa488 channel in green ($\lambda_{\mathrm{exc}} = 488$ nm; $\lambda_{\mathrm{em}} = 500$–$600$ nm), and (C) overlay image. Scale bars correspond to 100 μm. The sample was directly imaged without performing a centrifugation step.

(Table 1). Concomitantly, the molar fractions of membrane-bound Lz-A488 molecules in monomeric and hexameric form were calculated to decrease/increase from 0.23 to 0.10 and from 0.41 to 0.67, respectively. Since the free donors do not undergo in efficient Förster energy transfer to the fluorescently head labeled phospholipid used as the acceptor, their presence in solution must be accounted for in the data treatment to avoid getting underestimated FRET efficiencies.[28] In this case, free Lz-A488 includes all derivatized protein molecules that are not in direct contact (<2 Förster radius, R_0) with lipids. As described in detail in the ESI,† the interplanar FRET topological model (eqn (S10)†), corrected for the presence of isolated donors in solution (eqn (S8) and (S9)†), was globally fitted to a set of 3 fluorescence decays obtained for each protein concentration, namely the decay curves measured for Lz-A488 in aqueous solution ($I_D^w(t)$) and in the presence of 430 μM POPC : POPS 80 : 20 LUVs, including or not the acceptor ($I_{DA}(t)$ and $I_D(t)$, respectively). To improve the quality of the fits, several fitting parameters were either fixed (including x_D^w) or linked between the 3 decay curves under analysis (for more details, see ESI†). The fitted parameters recovered from these global analyses are summarized in Table 1. As expected, the mean fluorescence lifetime obtained for the membrane-bound Lz-A488, $\langle\tau\rangle_1^{D,m}$, was lower than the experimental $\langle\tau\rangle_1^D$ value (bulk measurements), and close to the mean value of the $\langle\tau\rangle_1^D$ histograms measured for the isolated fibers (Fig. 2D and Table S1†) and aggregates (Fig. S1 and Table S1†) using the FLIM methodology. These results are in line with the facts that (i) both aqueous and membrane-bound monomeric Lz-A488 present a longer mean fluorescence lifetime ($\langle\tau\rangle_1 = 3.0$ ns) than the membrane-bound oligomeric form of the conjugated protein ($\langle\tau\rangle_1 = 1.5$ ns)[15] and (ii) the predominant Lz-A488 membrane bound form in each sample is oligomeric. The donor–acceptor interplanar transverse distance, h, obtained for all the protein concentrations studied was ~2.5 nm (Table 1), as exemplified in Fig. S2.† More importantly, the energy transfer efficiencies corrected for the presence of free donors in solution, E_{FRET}^m, were much higher than the uncorrected FRET efficiencies, E_{FRET}^{bulk}, and became essentially independent of the donor concentration used in the assay, as expected. Strikingly, the average bulk $E_{FRET}^m = 0.31 \pm 0.02$ (mean ± SD) recovered for the 3 protein concentrations studied is now in good agreement with $E_{FRET}^{FLIM} = 0.36 \pm 0.03$ ($n = 3$) measured at the single-fiber, indicating that the time-resolved data were adequately corrected for the existence of free isolated donors. Finally, and as shown in Fig. 2B, both E_{FRET}^m and E_{FRET}^{FLIM} are also in good agreement with the interplanar energy transfer efficiency predicted in the presence of two instead of one acceptor plane (Fig. 2A) within a 2.5–3.0 nm distance of membrane-bound Lz-A488, showing that lysozyme is intercalated between two adjacent lipid bilayers. Eventually, it could be argued that the obtained results were compatible with lysozyme-bridged vesicle aggregation, with the latter essentially maintaining a bilayer structure. The reasoning behind this argument would be that the protein donors would only be sensing confined regions of lysozyme-induced contact between adjacent vesicles, where two planes of lipid acceptors (one in each of the adhering vesicles) would be available for FRET. Further from these regions, a single bilayer lipid arrangement would be kept. However, this scenario can be excluded taking into account our previous measurements of FRET between two lipid probes. Time-resolved FRET between 2-(4,4-difluoro-5-methyl-4-bora-3*a*,4*a*-diaza-*s*-indacene-3-dodecanoyl)-1-hexadecanoyl-*sn*-*glycero*-3-phosphocholine (BODIPY-PC) and Rh-PE inserted in POPC/POPS 80 : 20 vesicles, in the presence of unlabelled lysozyme, was significantly better described, both statistically (global χ^2) and in terms of the physical meaning of the fitting parameters (D decay in the absence of A, acceptor concentration) by allowing FRET to multiple planes of acceptors in the analysis model.[25] This study showed that lipid donors, which distribute in the entire bilayer and not solely near the sites of protein attachment, sense multiple planes of acceptors, and are indicative of extensive bilayer stacking.[25]

It is also important to draw here some brief considerations about the differences implemented in the analysis of the time-resolved fluorescence data performed in this work in comparison to the previous study.[25] Much better fittings of the theoretical FRET models to the experimental $I(t)$ data were now obtained by explicitly considering the presence of free donors in solution, as reported by a lower global chi-square of the fittings (compare Fig. S2† with Fig. 5B from ref. 25). However, the fittings still present a low sensitivity to the transverse distance between the donor and acceptor planes, h, particularly for low h values. Most probably, this result stems from the intrinsic heterogeneity in the donor population (co-existence of membrane-bound monomeric and hexameric Lz-A488 species; non-specific labeling of lysozyme), which is expected to broaden significantly the range of possible h values as mentioned before.[25] Nevertheless, the thickness of the interbilayer aqueous space, $\delta_w = 2 \times h \sim 5$–6 nm, recovered in this study is now closer to the value measured earlier by performing FRET measurements between two membrane probes (D = BODIPY-PC; A = Rh-PE) in the presence of lysozyme ($\delta_w = 6.7$ nm[25]). This

Table 1 Fitting parameters recovered from the individual and global analysis of the macroscopic (bulk) time-resolved FRET data

	Individual analysis[a]		Global analysis[b]					
[Lz-A488] (μM)	$\langle\tau\rangle_1^D$ (ns)	E_{FRET}^{bulk}	x_D^{wc}	$\langle\tau\rangle_1^{D,md}$ (ns)	h (nm)	C^e	E_{FRET}^m	χ_G^2
1.0	2.32	0.15	0.36	2.06	2.5	0.39	0.30	1.18
1.5	2.10	0.16	0.29	1.84	2.5	0.38	0.29	1.20
3.0	2.01	0.20	0.23	1.81	2.5	0.45	0.33	1.45

[a] For each protein concentration, $I_D(t)$ and $I_{DA}(t)$ were fitted to a sum of exponentials (eqn (S5)). [b] For each protein concentration, the fluorescence decays were globally analyzed considering the presence of free Lz-A488 in solution and the occurrence of interplanar energy transfer from the membrane-bound donor molecule to a plane of randomly distributed acceptors (Rh-PE) (eqn (S8)–(S12)). [c] The molar fraction of free donor molecules (Lz-A488) in solution was calculated independently using $k = 6$ and $K_{ag} = 2 \times 10^{14}$ according to the cooperative partition model developed earlier[15] and held fixed in the global fit. [d] Mean fluorescence lifetime calculated for the membrane-bound donors (excluding the contribution of free donors in aqueous solution) (eqn (S6)). [e] Acceptor numerical density (eqn (S11)).

interbilayer thickness is wide enough to accommodate monomeric, or even oligomeric, sideways-on or headways-on membrane-bound lysozyme molecules (the enzyme is a prolate ellipsoid 3.0 × 4.5 nm[29]), particularly if lysozyme partially penetrates the membrane surface at a high protein surface coverage.[30] Altogether, these complementary FRET results, performed both at the bulk (liposome ensemble-average) and microscopic (single-fiber/aggregate) levels, support the conclusion that both the lipid–protein mixed supramolecular assemblies formed upon lysozyme interaction with anionic phospholipid vesicles at a low L/P ratio display a multilayer structure, in which the predominantly hexameric lysozyme is sandwiched between two adjacent lipid bilayers.

FRAP analysis reveals reduced lateral mobility for lysozyme and phospholipids in the lipid–protein mixed fibers

After establishing that lysozyme induces the stacking of anionic lipid bilayers at a low L/P ratio, it was important to study the impact of fiber formation on the protein and lipid lateral dynamics. Toward this end, FRAP was employed to investigate the modifications in the lateral mobilities of Lz-NBD and two fluorescently lipid probes (NBD-PE and NBD-PS) embedded in these mesoscopic structures. FRAP is a standard technique that has been extensively used to measure the molecular mobility of lipids and proteins in membranes, allowing to gather information about *e.g.* lipid domain formation and protein oligomerization in the system under study.[31,32] As it is exemplified in Fig. 3A and B, and further confirmed by the normalized FRAP recovery curves obtained for the diffusion of Lz-NBD, NBD-PE (Fig. 3C) and NBD-PS incorporated in these mixed fibers, both lipid probes present much lower mobile fractions ($M_f = 0.11 \pm 0.01$, $n = 4$ and $= 0.20 \pm 0.02$, $n = 5$ for NBD-PE and NBD-PS, respectively) as compared to Lz-NBD ($M_f = 0.81 \pm 0.02$, $n = 5$) on the time scale of the FRAP experiments (Fig. 3E). However, the mobile fraction of Lz-NBD diffuses at the same rate, within error, as both fluorescent lipids, but with almost a 10-fold lower diffusion coefficient ($D = 0.2$–0.4 μm^2 s^{-1}) than the typical value exhibited by a phospholipid in a fluid lipid phase like in the top hemisphere of immobilized POPC GUVs ($D_{NBD\text{-}PE} = 2.7 \pm 0.4$ μm^2 s^{-1}, $n = 17$ and $D_{NBD\text{-}PS} = 2.8 \pm 0.3$ μm^2 s^{-1}, $n = 12$) (Fig. 3D).[33] The lateral mobility features (diffusion coefficient and mobile fractions) displayed by Lz-NBD and both NBD-fluorescently labeled phospholipids within the mixed lipid–protein aggregates studied were again essentially identical to the ones just described for the fibers (data not shown). In each case, the good fits of the classic fluorescence recovery model to the experimental data show that the lateral translational dynamics of both the fluorescently labeled protein and phospholipids were well described by a single diffusion coefficient.

The pronounced reduction of lysozyme lateral diffusion coefficient when incorporated into these mesoscopic structures, as compared to the value presented by free-diffusing protein molecules ($D = 93 \pm 8$ μm^2 s^{-1}),[12] cannot be explained by the simple adsorption of a peripheral protein on the surface of the lipid vesicles. When a protein is tightly bound to a membrane–lipid component, its diffusion rate should decrease to a limiting value close to that of the phospholipid in a fluid–lipid phase.[34,35] Upon the establishment of a large number of interactions with multiple anionic lipids and/or significant bilayer penetration of the protein, a further slowdown of the diffusion of the membrane-bound system is expected to occur.[35] Therefore, the lateral diffusion of a protein is highly sensitive to the establishment of protein–lipid contacts.[31,34–36] According to the

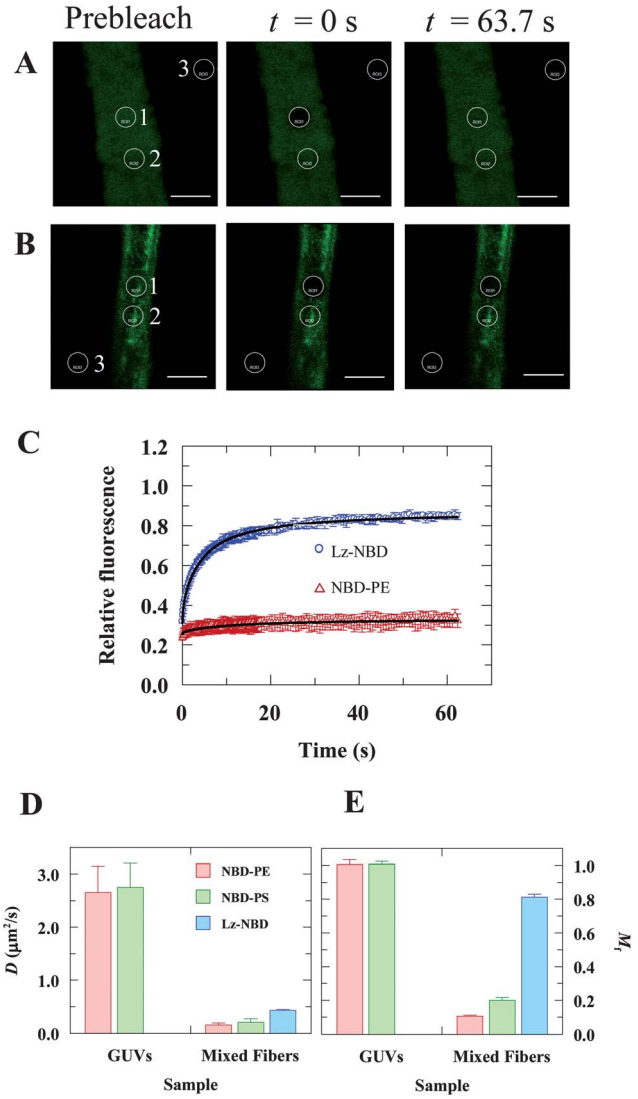

Fig. 3 Lateral diffusion of lysozyme and phospholipids is highly restricted in the lipid–protein mixed fibers. (A and B) Typical images of the lipid–protein mixed fibers before the bleach, immediately after the bleach ($t = 0$ s), and after recovery of fluorescence for the diffusion of (A) Lz-NBD and (B) NBD-PE. The circular regions 1, 2 and 3 correspond to the bleached, the reference and background regions of interest (ROIs), respectively. The scale bars represent 10 μm. (C) Normalized FRAP curves obtained for the diffusion of Lz-NBD and NBD-PE in the lipid–protein mixed fibers. The data represent the mean ± standard deviation (SD) of 4–5 FRAP experiments. The solid lines are the best nonlinear fits of eqn (S2)† to the experimental data. (D) Diffusion coefficients, D, and (E) mobile fractions, M_f, measured for NBD-PE, NBD-PS and Lz-NBD in POPC GUVs and the lipid–protein mixed fibers. The error bars denote the standard deviation of the recovered parameters.

discussion above, the very slow diffusion of both Lz-NBD and the fluorescent lipid probes on these lipid–protein fibers must result from the interplay of two different factors. On one hand, the high surface coverage by lysozyme, which is expected to drive its oligomerization in the membrane,[15] must influence its lateral mobility. Indeed, the effect of membrane surface crowding of the adsorbed protein on lipid and protein lateral diffusion has been extensively studied for the interaction of annexins with negatively charged supported lipid bilayers (SLBs) containing either phosphatidylserine or phosphatidylglycerol.[31,36] The authors of these reports have shown that there was a strong reduction in both the lateral motion of the lipids and the protein itself upon increasing the surface occupancy of the SLBs.[31,36] Lysozyme assembly after its binding to the anionic lipid membranes might have also caused a tighter molecular packing of the phospholipids at the surface of the membranes, decreasing the lateral mobility of both Lz-NBD and the fluorescently labeled phospholipids studied. On the other hand, the drastic reduction of the lateral mobility of Lz-NBD may also be induced by protein confinement due to the formation of multilamellar structures, in which the oligomeric protein is sandwiched between adjacent lipid bilayers (see previous section).[37] Finally, since each lysozyme molecule binds to multiple phospholipids in the same or adjacent bilayers, it is not surprising that much lower phospholipid mobile fractions were recovered as compared to the one obtained for Lz-NBD (Fig. 3E).

Laurdan fluorescence reports changes in the interfacial hydration/lateral lipid packing in the lipid–protein mixed fibers

The next step of this study was to clarify whether the formation of these lipid–protein mixed fibers exerted a strong impact on the interfacial properties of the lipid membranes. In this way, 1PE and 2PE measurements of the GP of the fluorescent lipid probe Laurdan[16,38] were again performed at the ensemble (bulk) and single fiber level, respectively. Laurdan exhibits extreme sensitivity to the membrane polarity and the dipolar relaxation of this probe in the lipid membrane produces spectral shifts in its emission spectrum which can be quantified by calculating the empirical function called GP (eqn (1)).[23,38] The GP values of Laurdan are high when no relaxation occurs, and since the main solvent dipoles surrounding Laurdan in phospholipid membranes are water molecules, a high GP value reports a low water content/mobility at the interface region.[38] On the other hand, if the membrane interface is highly hydrated, the emission spectrum of Laurdan strongly shifts to red and a low GP value is recovered.[38] As the transition from a liquid crystalline to a gel phase membrane is accompanied by an increased molecular packing of the phospholipids, which decreases the water penetration and dynamics at the interface region, the GP parameter has most often been used as a reporter of the membrane order.[16,38] As illustrated in Fig. 4A, the pseudo-colored 2PE fluorescence microscopy images obtained for control POPC GUVs and the lipid–protein mixed fibers present a rather homogeneous distribution of GP values in both cases. Interestingly, however, the resulting histograms were quite different as the distribution obtained for the mixed fibers was centered at a much higher value ($GP^{mean}_{micro} = 0.63 \pm 0.05$, $n = 5$) as compared to the control POPC GUVs ($GP^{mean}_{micro} = 0.09 \pm 0.02$, $n = 5$) (Fig. 4A and B). On the other hand, the GP histogram obtained for DOPC : DPPC 50 : 50 GUVs, which present gel-fluid co-existing lipid domains,[16] was best described by a bimodal Gaussian distribution (Fig. 4B), confirming the ability of these microscopic measurements to detect lateral micro heterogeneity in the supramolecular assembly under study. Moreover, although the bulk (1PE) and micro (2PE) control GP values measured for different lipid mixtures studied agreed reasonably well with each other, as expected, the GP^{mean}_{micro} of the mixed fibers at the microscopic level was much higher than the one measured in the spectrofluorometer for the ensemble average population obtained following the addition of 3 μM lysozyme to 430 μM POPC : POPS 80 : 20 LUVs ($GP_{bulk} = 0.00 \pm 0.03$, $n = 3$) (Fig. 4C). Altogether, these results clearly demonstrate that the formation of the lipid–protein mixed fibers, which correspond to a small subpopulation of the sample, is accompanied by an extensive dehydration of the membrane interface and/or increased interfacial phospholipid packing, at variance with what occurs in the mixed lipid–protein aggregates. Interestingly, this is a spectroscopic signature shared by several

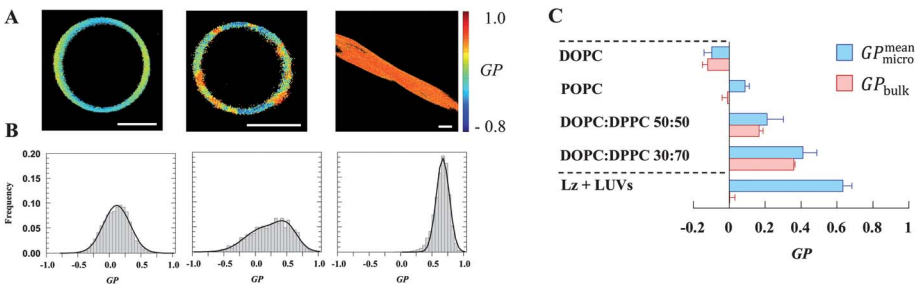

Fig. 4 Lipid–protein mixed fiber formation has a strong impact on the head group hydration/lateral packing of the membrane interface. (A) Typical Laurdan pseudo-colored GP images and (B) associated histograms obtained for POPC GUVs, DOPC : DPPC 50 : 50 GUVs and the lipid–lysozyme mixed fibers (from left to right, respectively). GUV images show equatorial sections. The colors indicate different GP values following the reported scale. Scale bars represent 10 μm. (C) Comparison between bulk (1PE) and microscopic (2PE) mean GP values obtained from ensemble average and single GUV/fiber measurements, respectively, for the different systems studied prepared with the lipid compositions indicated. Lz + LUVs designate the sample obtained upon incubation of 3 μM lysozyme with 430 μM POPC : POPS 80 : 20 LUVs.

cochleate structures produced upon the interaction of Ca^{2+} [39] ions and several polycationic molecules (*e.g.* polylysine[40] and several antimicrobial oligo-acyl-lysyls peptides (OAKs)[41–43]) with liposomes prepared with either acidic phospholipids (usually PS) or different lipid mixtures of zwitterionic and anionic phospholipids. In fact, Laurdan fluorescence has been proposed as a useful method to detect the formation of cochleates since the fluorescence properties of Laurdan embedded in these mesoscopic structures are quite distinct from those observed in gel and liquid-crystalline phases and consistent with a more dehydrated and rigid membrane interface.[44] Taking into account both the FRET and GP results, together with their morphological features, we speculate that the lipid–protein mixed fibers studied here might correspond to multilamellar folded cochleate structures formed by the spiraling of the fused lipid bilayer sheets cross-bridged by lysozyme. In this regard, it should be noted that the aqueous spaces within the Ca^{2+}-bridged cochleates can accommodate several drugs and proteins (like amphotericin B and recombinant Factor VIII[45]). On the other hand, previous studies have already reported that the electrostatic interaction of the highly cationic lysozyme with negatively charged membranes was able to induce an extensive dehydration of the membrane surface. These bulk studies, which were based on exploring the fluorescence properties of dansyl-phosphatidylethanolamine that strongly depend on the dielectric properties of the membrane interface,[46] were carried out with vesicles containing a high mol% of the negatively charged phospholipid and at a more acidic pH.[47] Both these conditions are expected to maximize the electrostatic interactions at play and therefore must increase the probability of obtaining and detecting these dehydrated structures under bulk conditions.

Membrane-bound lysozyme incorporated in the supramolecular assemblies formed at a low L/P ratio does not display amyloid (β-sheet) characteristics

Finally, we assessed whether lysozyme binding to 20 mol% POPG-containing POPC LUVs was able to prompt the conformational transition of the protein into a β-sheet rich structure (which characterizes amyloid fibril formation), as proposed in the literature.[6] To address this question, IR spectroscopy was used since this spectroscopic technique is more sensitive to the β-sheet content of a protein and less affected by the sample scatter as compared to circular dichroism. POPG replaced POPS as the anionic phospholipid used in the preparation of the lipid vesicles in these experiments to avoid the interference from the antisymmetric amine-NH_3^+ and carboxylate stretch of PS in the IR spectra of the protein.[48] The pellet obtained after a centrifugation step of the lipid–protein supramolecular assemblies produced upon incubating 70 μM of lysozyme in D_2O buffer with 10 mM POPC : POPG 80 : 20 LUVs was now used in these spectroscopic measurements to minimize the contribution of free protein to the IR spectra (the L/P molar ratio of the sample was kept constant).

The secondary structure content of lysozyme in aqueous solution and embedded in these supramolecular complexes was investigated by analyzing the amide I′ band, in the spectral range 1700–1600 cm^{-1}. As shown in Fig. S3A and B,† the amide I′ bands were deconvoluted into five main components, each of which can be associated with specific elements of the secondary structure. The bands centered at 1685 and 1672 cm^{-1} are characteristic of β-turns, that at 1655 cm^{-1} are assigned to the α-helix, and finally, those at 1639 and 1623 cm^{-1} correspond to β-sheets.[49] As expected for lysozyme in solution, a dominant band at 1655 cm^{-1} (41%) (Table 2) was observed, which reflects a large α-helical component in the soluble native protein.[50,51] Notably, the amide I′ band of lysozyme in the supramolecular assemblies was not significantly different from that found for lysozyme in aqueous solution, since a dominant band with a maximum frequency at 1655 cm^{-1} (37%) also appeared in this case (Table 2). Upon analyzing the IR spectrum in this region in more detail, only a slight decrease of α-helix (4%) and β-turn (3%) content and a concomitant increase of β-sheets (7%) was obtained for lysozyme embedded in these mixed supramolecular assemblies. Therefore, these results show that lysozyme displays a nearly native structure in the electrostatically driven lipid–protein complexes formed, and no extensive lipid-mediated conformational-transition of lysozyme into a β-sheet rich structure (typical of amyloid fibril formation) was detected under the conditions used in this study.

It is important to mention that although our IR measurements were not conducted at the microscopic level, this has already been done in a previous study of the "amyloid-like" fibers produced upon interaction of cytochrome c (a protein with a similar size and net charge to lysozyme) with anionic liposomes.[52] By employing IR microscopy, the authors were also unable to detect an extensive structural re-arrangement of this protein within the individual fibers or sections of fibers examined since only some of the bluish fibers studied displayed IR bands that are typically attributed to amyloid β-sheet structures. More recently, lysozyme has also been proposed to unfold in contact with lipid membranes and grows into amyloid fibrils upon incubation with POPG GUVs.[13,14] However, the conditions used in these studies were quite different from our work since a much higher anionic lipid content and prolonged incubation times (up to several days) were employed. In addition, this conclusion strongly relied on thioflavin T and Congo Red binding assays to detect amyloid formation, although both these dyes are capable of producing false positive results, particularly in the presence of anionic membranes.[53,54] Other

Table 2 Deconvolution of amide I′ band of lysozyme in solution or embedded in the supramolecular assemblies formed upon lysozyme interaction with anionic membranes at a low L/P ratio

Band (cm^{-1})	Assigned secondary structure	Buffer[a] (area%)	Supramolecular assemblies (area%)
1685	β-Turn	3	2
1672	β-Turn	16	14
1655	α-Helix	41	37
1639	Intramolecular β-sheet	34	39
1623	Intermolecular β-sheet	6	8

[a] D_2O buffer (20 mM HEPES–KOH, 0.1 mM EDTA, pD 7.4 buffer).

studies have shown that hen egg-white lysozyme can indeed form amyloid fibrils *in vitro* but only upon prolonged incubation under a variety of strongly destabilizing conditions (*e.g.* low pH (pH 1.6–3.0) and elevated temperature (55–80 °C) or in the presence of high concentrations of ethanol (for a critical review see ref. 55)).

Conclusions

In summary, we have applied a toolbox of complementary biophysical methodologies to gain an increased understanding about the supramolecular assemblies produced upon lysozyme interaction with POPC : POPS 80 : 20 LUVs at a low L/P molar ratio and using a low ionic strength medium. A careful microscopic characterization of the samples revealed that they were highly polymorphic, although mixed lipid–protein fibers could always be easily distinguished from the more abundant and irregularly shaped lipid–protein aggregates. When possible, microscopic measurements performed individually at the single-fiber/aggregate level were compared with the bulk (ensemble average) measurements to retrieve important information regarding the possible heterogeneity in the structural and dynamic properties of the morphologically distinct components of the sample.

Since the structural details of the lipid–protein complexes are on a length scale below the resolution of optical microscopy, an established fluorescence spectroscopy technique, FRET, was first used to perform a molecular topography imaging of these fibers. By taking full advantage of the FRET sensitivity to distance, and by employing advanced formalisms for FRET kinetics analysis already applied in several membrane studies,[25,56,57] we concluded that both the lipid–protein mixed fibers and aggregates presented a multilayer structure, whereupon the predominantly oligomeric membrane-bound Lz-A488 is intercalated between adjacent lipid bilayers. Additionally, as shown by FRAP, the extensive protein oligomerization produced at high membrane surface crowding and/or protein confinement between the cross-bridged bilayers, imposed a slow lateral diffusion of the fluorescently labeled lysozyme in these mesoscopic structures. In fact, although Lz-NBD diffused laterally at the same rate in these mixed fibers as both the fluorescently lipid probes studied (NBD-PE and NBD-PS), they displayed an almost 10-fold lower diffusion coefficient ($D = 0.2$–$0.4\ \mu m^2\ s^{-1}$) than the typical value exhibited by a phospholipid in a fluid lipid phase. Laurdan, a fluorescent membrane probe that is localized at the interface between the polar glycerol head group and the acyl chains of phospholipids, was then used to report structural perturbations occurring at the membrane surface upon lysozyme binding. The most distinctive result of this study was the finding that the lipid–lysozyme mixed fibers formed under the conditions used presented a GP_{micro}^{mean} value much higher than the value measured for the bulk sample, GP_{bulk}. Strikingly, this result shows that the formation of these mesoscopic structures produces a highly dehydrated/rigid environment at the membrane interface, at variance with what occurs with the major components (aggregates) of the sample. We speculate that the lipid–protein mixed "amyloid-like" fibers are cochleate cylindrical structures with lysozyme acting as the inter-layer cross-bridging agent. Finally, IR bulk measurements carried out with the pellet resulting from the interaction of lysozyme with the 20 mol%-POPG containing POPC lipid vesicles only detected minor alterations in the secondary structure content of the protein, ruling out the hypothesis that anionic liposomes can mediate an extensive conformational-transition of lysozyme into a β-sheet rich-structure.

Changes in the liposome/membrane morphology in response to protein binding result from a delicate balance between the binding interactions established (electrostatic and/or hydrophobic), mechanical properties (membrane elasticity), and molecular geometries of its components (lipids and proteins).[58] The lipid–protein mixed supramolecular assemblies studied here exhibited a variety of forms. Although clearly the changes produced on the membrane architecture of the liposomes (a soft interface) upon lysozyme binding are always primarily driven by electrostatic interactions,[10–14] the fine molecular details of this process have to be sufficiently different (either thermodynamically and/or kinetically) to produce distinct final mesoscopic structures, fibers and aggregates, respectively. Intriguingly, other than their morphological features, a change in surface dehydration/molecular packing at the membrane interface was the only molecular property that could be individually resolved within the mixed population of lipid–protein complexes studied here. Accordingly, this change in the membrane interfacial properties is also probably the key event triggering the final adoption of the fiber morphology by the lipid–lysozyme supramolecular complexes. At this point, we can only speculate about the factors that control this process. Probably, high local initial concentrations of lysozyme resulting from its introduction into the liposome suspension must modulate the protein-induced lipid vesicle aggregation and fusion process, changing the final membrane properties of the mixed lipid–protein complexes formed. Eventually, transient electrostatically induced clustering of the anionic lipids into nanoscopic membrane domains by lysozyme might locally change the membrane hydration and curvature. In fact, the energy required for membrane bending is expected to be the dominant barrier for mixed lipid–protein fiber formation, controlling the lysozyme-induced wrapping of the fused lipid membranes. A significant contribution from entropy to the free energy of this process is expected to result from the release of hydrated water from the phospholipid head groups upon extensive lysozyme binding and oligomerization on the membrane surface at a low L/P molar ratio.[15]

In conclusion, results reported herein provide new structural insights into the molecular properties displayed by the lipid–protein mixed "amyloid-like" fibers, showing that negatively charged membranes do not have the general ability to trigger amyloid fibril formation of non-amyloidogenic proteins, at variance with a previous report.[6]

Acknowledgements

We thank Dr Aleksander Fedorov for performing the time-resolved (bulk) fluorescence measurements and Sandra Pinto

for her assistance in the two-photon microscopic studies of Laurdan. A.M. and F.F. acknowledge the support of Fundação para a Ciência e Tecnologia (FCT) *via* SFRH/BD/61723/2009 and SFRH/BPD/64320/2009 grants, respectively. This work was supported by projects PTDC/QUI-BIQ/099947/2008 and PTDC/BBB-BQB/2661/2012 from FCT.

References

1 C. Aisenbrey, T. Borowik, R. Bystrom, M. Bokvist, F. Lindstrom, H. Misiak, M. A. Sani and G. Grobner, *Eur. Biophys. J. Biophys. Lett.*, 2008, **37**, 247–255.
2 J. A. Hebda and A. D. Miranker, *Annu. Rev. Biophys.*, 2009, **38**, 125–152.
3 R. Kayed, Y. Sokolov, B. Edmonds, T. M. McIntire, S. C. Milton, J. E. Hall and C. G. Glabe, *J. Biol. Chem.*, 2004, **279**, 46363–46366.
4 G. P. Gorbenko and P. K. J. Kinnunen, *Chem. Phys. Lipids*, 2006, **141**, 72–82.
5 S. M. Butterfield and H. A. Lashuel, *Angew. Chem., Int. Ed.*, 2010, **49**, 5628–5654.
6 H. X. Zhao, E. K. J. Tuominen and P. K. J. Kinnunen, *Biochemistry*, 2004, **43**, 10302–10307.
7 H. X. Zhao, A. Jutila, T. Nurminen, S. A. Wickstrom, J. Keski-Oja and P. K. J. Kinnunen, *Biochemistry*, 2005, **44**, 2857–2863.
8 C. Code, Y. Domanov, A. Jutila and P. K. J. Kinnunen, *Biophys. J.*, 2008, **95**, 215–224.
9 A. K. Mahalka and P. K. J. Kinnunen, *Biochim. Biophys. Acta, Biomembr.*, 2009, **1788**, 1600–1609.
10 J. J. Bergers, M. H. Vingerhoeds, L. Vanbloois, J. N. Herron, L. H. M. Janssen, M. J. E. Fischer and D. J. A. Crommelin, *Biochemistry*, 1993, **32**, 4641–4649.
11 O. Zschornig, G. Paasche, C. Thieme, N. Korb and K. Arnold, *Colloids Surf., B*, 2005, **42**, 69–78.
12 A. M. Melo, M. Prieto and A. Coutinho, *Biochim. Biophys. Acta, Biomembr.*, 2011, **1808**, 2559–2568.
13 T. Al Kayal, S. Nappini, E. Russo, D. Berti, M. Bucciantini, M. Stefani and P. Baglioni, *Soft Matter*, 2012, **8**, 4524–4534.
14 T. Al Kayal, E. Russo, L. Pieri, G. Caminati, D. Berti, M. Bucciantini, M. Stefani and P. Baglioni, *Soft Matter*, 2012, **8**, 9115–9126.
15 A. M. Melo, J. C. Ricardo, A. Fedorov, M. Prieto and A. Coutinho, *J. Phys. Chem. B*, 2013, **117**, 2906–2917.
16 T. Parasassi, E. Gratton, W. M. Yu, P. Wilson and M. Levi, *Biophys. J.*, 1997, **72**, 2413–2429.
17 C. W. F. McClare, *Anal. Biochem.*, 1971, **39**, 527–530.
18 *The Handbook. A Guide to Fluorescent Probes and Labeling Technologies*, ed. R. P. Haugland, Molecular Probes, Eugene, OR, 10th edn, 2005.
19 J. D. Shore, D. E. Day, A. M. Francischmura, I. Verhamme, J. Kvassman, D. A. Lawrence and D. Ginsburg, *J. Biol. Chem.*, 1995, **270**, 5395–5398.
20 C. N. Pace, F. Vajdos, L. Fee, G. Grimsley and T. Gray, *Protein Sci.*, 1995, **4**, 2411–2423.
21 S. N. Pinto, L. C. Silva, R. F. M. de Almeida and M. Prieto, *Biophys. J.*, 2008, **95**, 2867–2879.
22 M. J. Sarmento, M. Prieto and F. Fernandes, *Biochim. Biophys. Acta, Biomembr.*, 2012, **1818**, 2605–2615.
23 D. M. Owen, C. Rentero, A. Magenau, A. Abu-Siniyeh and K. Gaus, *Nat. Protoc.*, 2012, **7**, 24–35.
24 F. Waharte, K. Steenkeste, R. Briandet and M. P. Fontaine-Aupart, *Appl. Environ. Microbiol.*, 2010, **76**, 5860–5869.
25 A. Coutinho, L. M. S. Loura, A. Fedorov and M. Prieto, *Biophys. J.*, 2008, **95**, 4726–4736.
26 A. Bernabeu, J. Guillen, A. J. Perez-Berna, M. R. Moreno and J. Villalain, *Biochim. Biophys. Acta, Biomembr.*, 2007, **1768**, 1659–1670.
27 M. Giudici, R. Pascual, L. de la Canal, K. Pfuller, U. Pfuller and J. Villalain, *Biophys. J.*, 2003, **85**, 971–981.
28 *Principles of fluorescence spectroscopy*, ed. Lakowicz, Springer, New York, 2006.
29 C. C. F. Blake, D. F. Koenig, G. A. Mair, A. C. T. North, D. C. Phillips and V. R. Sarma, *Nature*, 1965, **206**, 757–761.
30 B. Yuan, L. L. Xing, Y. D. Zhang, Y. Lu, Y. Y. Luo, Z. H. Mai and M. Li, *J. Phys. Chem. B*, 2007, **111**, 6151–6155.
31 L. Cezanne, A. Lopez, F. Loste, G. Parnaud, O. Saurel, P. Demange and J. F. Tocanne, *Biochemistry*, 1999, **38**, 2779–2786.
32 D. M. Owen, D. Williamson, C. Rentero and K. Gaus, *Traffic*, 2009, **10**, 962–971.
33 L. Guo, J. Y. Har, J. Sankaran, Y. M. Hong, B. Kannan and T. Wohland, *ChemPhysChem*, 2008, **9**, 721–728.
34 J. D. Knight and J. J. Falke, *Biophys. J.*, 2009, **96**, 566–582.
35 J. D. Knight, M. G. Lerner, J. G. Marcano-Velazquez, R. W. Pastor and J. J. Falke, *Biophys. J.*, 2010, **99**, 2879–2887.
36 R. Gilmanshin, C. E. Creutz and L. K. Tamm, *Biochemistry*, 1994, **33**, 8225–8232.
37 M. Reffay, Y. Gambin, H. Benabdelhak, G. Phan, N. Taulier, A. Ducruix, R. S. Hodges and W. Urbach, *PLoS One*, 2009, **4**, 1–9.
38 T. Parasassi, G. De Stasio, G. Ravagnan, R. M. Rusch and E. Gratton, *Biophys. J.*, 1991, **60**, 179–189.
39 D. Papahadjopoulos, W. J. Vail, K. Jacobson and G. Poste, *Biochim. Biophys. Acta*, 1975, **394**, 483–491.
40 U. M. Syed, A. F. Woo, F. Plakogiannis, T. Jin and H. Zhu, *Int. J. Pharm.*, 2008, **363**, 118–125.
41 L. Livne, R. F. Epand, B. Papahadjopoulos-Sternberg, R. M. Epand and A. Mor, *Faseb J.*, 2010, **24**, 5092–5101.
42 R. F. Epand, H. Sarig, D. Ohana, B. Papahadjopoulos-Sternberg, A. Mor and R. M. Epand, *J. Phys. Chem. B*, 2011, **115**, 2287–2293.
43 H. Sarig, D. Ohana, R. F. Epand, A. Mor and R. M. Epand, *Faseb J.*, 2011, **25**, 3336–3343.
44 K. Ramani and S. V. Balasubramanian, *Biochim. Biophys. Acta, Biomembr.*, 2003, **1618**, 67–78.
45 R. D. Miclea, P. R. Varma, A. Peng and S. V. Balu-Iyer, *Biochim. Biophys. Acta, Biomembr.*, 2007, **1768**, 2890–2898.
46 S. Ohki and K. Arnold, *Methods Enzymol.*, 2003, **367**, 253–272.
47 O. Zschornig, G. Paasche, C. Thieme, N. Korb, A. Fahrwald and K. Arnold, *Gen. Physiol. Biophys.*, 2000, **19**, 85–101.
48 L. K. Tamm and S. A. Tatulian, *Q. Rev. Biophys.*, 1997, **30**, 365–429.
49 J. L. R. Arrondo, A. Muga, J. Castresana and F. M. Goni, *Prog. Biophys. Mol. Biol.*, 1993, **59**, 23–56.

50 D. M. Byler and H. Susi, *Biopolymers*, 1986, **25**, 469–487.
51 A. Dong, P. Huang and W. S. Caughey, *Biochemistry*, 1990, **29**, 3303–3308.
52 J. M. Alakoskela, A. Jutila, A. C. Simonsen, J. Pirneskoski, S. Pyhajoki, R. Turunen, S. Marttila, O. G. Mouritsen, E. Goormaghtigh and P. K. J. Kinnunen, *Biochemistry*, 2006, **45**, 13447–13453.
53 R. Khurana, V. N. Uversky, L. Nielsen and A. L. Fink, *J. Biol. Chem.*, 2001, **276**, 22715–22721.
54 S. Kumar, A. K. Singh, G. Krishnamoorthy and R. Swaminathan, *J. Fluoresc.*, 2008, **18**, 1199–1205.
55 A. J. Trexler and M. R. Nilsson, *Curr. Protein Pept. Sci.*, 2007, **8**, 537–557.
56 C. Madeira, L. M. S. Loura, M. R. Aires-Barros, A. Fedorov and M. Prieto, *Biophys. J.*, 2003, **85**, 3106–3119.
57 L. M. S. Loura, A. Coutinho, A. Silva, A. Fedorov and M. Prieto, *J. Phys. Chem. B*, 2006, **110**, 8130–8141.
58 H. T. McMahon and J. L. Gallop, *Nature*, 2005, **438**, 590–596.